Optimizing synchronization stability of the Kuramoto model in complex networks and power grids

Bo Li and K. Y. Michael Wong
Department of Physics, The Hong Kong University of Science and Technology, Hong Kong
(Received 19 August 2016; revised manuscript received 7 December 2016; published 13 January 2017)

Maintaining the stability of synchronization state is crucial for the functioning of many natural and artificial systems. In this study, we develop methods to optimize the synchronization stability of the Kuramoto model by minimizing the dominant Lyapunov exponent. Using the recently proposed cut-set space approximation of the steady states, we greatly simplify the objective function, and further derive its gradient and Hessian with respect to natural frequencies, which leads to an efficient algorithm with the quasi-Newton's method. The optimized systems are demonstrated to achieve better synchronization stability for the Kuramoto model with or without inertia in certain regimes. Hence our method is applicable in improving the stability of power grids. It is also viable to adjust the coupling strength of each link to improve the stability of the system. Various operational constraints can also be easily integrated into our scope by employing the interior point method in convex optimization. The properties of the optimized networks are also discussed.

DOI: 10.1103/PhysRevE.95.012207

I. INTRODUCTION

Synchronization occurs widely in many natural and artificial systems, such as firefly flashes, pacemaker cells of heart, Josephson junctions, and power grids [1–4]. In general, the synchronous states are subject to different kinds of perturbations, and maintaining the stability of the systems against these perturbations is crucial for the functioning of the systems under consideration. For instance, the power grids are subject to various disturbances and real-time active controls are needed to maintain a stable synchronization state [4]. The future power grids will sustain larger and larger fluctuations with the introduction of more and more renewable energies such as wind and solar power, which raise needs to enhance the robustness and stability of existing power networks [5].

To describe these synchronization phenomena, statistical physicists have proposed many simple but explanatory models, e.g., chaotic oscillator systems, the Kuramoto model, and their various generalizations [3,6–8]. A remarkable relation between spectral aspects of network structure and synchronizability in a broad range of coupled oscillator models has been developed in the master stability function (MSF) framework [7,9]. In particular, the second smallest eigenvalues of the graph Laplacian matrix λ_2, namely the graph algebraic connectivity, is crucial in the synchronizability of models with unbounded MSF [7]. The graph algebraic connectivity is an interesting measure of network connectivity [10,11], whose role in dynamical stability can be exemplified in consensus dynamics or diffusion on networks $\dot{x}_i = -\sum_j L_{ij}x_j$, where λ_2 determines the rate of convergence of the slowest mode [7]. The graph algebraic connectivity is solely determined by the network topology. However, in many networks such as the power grid and transportation networks, stable behavior also depends on attributes other than topology.

In this study, we focus on the stability of the Kuramoto model on general networks. Due to the heterogeneity of power supply and demand, the stability of the frequency synchronization state of this nonlinear dynamical model is no longer determined by the graph algebraic connectivity or network structure itself, but is replaced by an algebraic connectivity that has an intricate dependence on the system steady state [12]. The optimization of synchronization stability should take into account both the graph connectivity and the dynamical parameters.

Enhancing the synchronization stability in these settings has been stressed in a few recent studies [13,14], where the effects of network structures or power grid parameters, e.g., the damping coefficients and power injections, on the system stability were explored. However, a practical consideration in implementing real-time flow control of the networks is the efficiency in calculating the gradient of the objective function in the space of variables, as was done in the cases of power scheduling and line impedance modification in power grids. Conventionally this requires us to solve the nonlinear flow equations in each update step, seriously slowing down the process. In this paper, we introduce the cut-set space approximation [15], enabling us to express the objective function in terms of the graph algebraic connectivity, thereby saving the need for the stepwise solution of the nonlinear flow equation and greatly simplifying the calculation of power flow and the evaluation of the gradients of the objective function.

II. THE MODEL

A. First-order Kuramoto model

We focus on the nonuniform first-order Kuramoto model on a connected network in the form of

$$\dot{\theta}_i = \omega_i + \sum_j K_{ij} \sin(\theta_j - \theta_i), \tag{1}$$

where θ_i denotes the phase angle of node i, ω_i the natural frequency, and $K_{ij}(=K_{ji})$ the coupling strength between node i and node j. Without loss of generality, we assume $\sum_i \omega_i = 0$. The steady state is given by

$$0 = \omega_i + \sum_j K_{ij} \sin(\theta_j^* - \theta_i^*). \tag{2}$$

In the leading order, the small deviation from the steady state $\delta\theta_i = \theta_i - \theta_i^*$ follows [12]

$$\delta\dot{\theta}_i \approx \sum_j K_{ij}\cos(\theta_j^* - \theta_i^*)(\delta\theta_j - \delta\theta_i) = -\sum_j L(\theta^*)_{ij}\delta\theta_j,$$

where $L(\theta^*)_{ij} := \delta_{ij}\sum_l K_{il}\cos(\theta_l^* - \theta_i^*) - K_{ij}\cos(\theta_j^* - \theta_i^*)$ is a state-dependent Laplacian matrix with edge weight $W(\theta^*)_{ij} = K_{ij}\cos(\theta_j^* - \theta_i^*)$. Note that this Laplacian matrix depends on the steady state of the system, in contrast with the state-independent Laplacian, which we denote as $L[K]_{ij} := \delta_{ij}\sum_l K_{il} - K_{ij}$. The Jacobian matrix is $J = -L(\theta^*)$, which has a null-space of dimension one, corresponding to the rotational symmetry of the model. If $|\theta_j^* - \theta_i^*| < \pi/2$ holds for every edge (i,j), then all the edge weights W_{ij} are positive and the lowest eigenvalue is 0, corresponding to the mode of uniform displacement. All the other eigenvalues of $L(\theta^*)$ are positive, making the dynamical system locally exponentially stable. In this case, the slowest mode corresponds to the second lowest eigenvalue of $L(\theta^*)$, that is, the negative of the largest Lyapunov exponent excluding the null exponent of J. We denote it as $\lambda_2(L(\theta^*))$ and call it the *state algebraic connectivity* to distinguish it from the usual *graph algebraic connectivity* $\lambda_2(L[K])$. To improve the stability, our objective is to maximize $\lambda_2(L(\theta^*))$ as in Ref. [13].

B. Second-order Kuramoto model

The second-order Kuramoto model is gaining attention due to its resemblance to the swing equation of power grids neglecting the transmission losses [12],

$$M_i\ddot{\theta}_i + D_i\dot{\theta}_i = P_i + \sum_j \frac{|V_i||V_j|}{X_{ij}}\sin(\theta_j - \theta_i), \qquad (3)$$

where M_i and D_i are the inertia and damping coefficient of node i, respectively, P_i and $|V_i|$ are the mechanical power and voltage magnitude of node i, and X_{ij} is the line reactance of edge (i,j). The connection to the Kuramoto model is obvious if P_i is identified as the natural frequency ω_i and $|V_i||V_j|/X_{ij}$ is identified as coupling K_{ij}. For simplicity, we consider uniform inertia and damping coefficient $M_i = M$ and $D_i = D$ and focus on the following model:

$$M\ddot{\theta}_i + D\dot{\theta}_i = \omega_i + \sum_j K_{ij}\sin(\theta_j - \theta_i). \qquad (4)$$

The steady state $(\dot{\theta}^* = 0, \theta^*)$ is again given by Eq. (2), with the Jacobian matrix evaluated at this point as [13,14]

$$J(\dot{\theta}^* = 0, \theta^*) = \begin{bmatrix} -\frac{D}{M}I & -\frac{1}{M}L(\theta^*) \\ I & 0 \end{bmatrix}.$$

As derived in Ref. [14], $J(\dot{\theta}^*, \theta^*)$ can be diagonalized by the eigenvectors of $L(\theta^*)$, with corresponding eigenvalues

$$\mu_{j\pm}(\lambda_j, D, M) = -\frac{D}{2M} \pm \frac{1}{2}\sqrt{\left(\frac{D}{M}\right)^2 - \frac{4}{M}\lambda_j(L(\theta^*))}. \qquad (5)$$

The maximal nontrivial eigenvalue is $\mu_{2+} = -\frac{D}{2M} + \frac{1}{2}\sqrt{(\frac{D}{M})^2 - \frac{4}{M}\lambda_2(L(\theta^*))}$. When $\lambda_2(L(\theta^*)) < D^2/4M$, improving $\lambda_2(L(\theta^*))$ will always lead to the increment of μ_{2+}. In this regime, optimizing $\lambda_2(L(\theta^*))$ is also applicable to stabilizing the uniform second-order Kuramoto model, therefore it can be applied in the stabilization of power grids. This regime can correspond to large damping, small inertia, or close to bifurcation.

III. METHOD

A. Variation of state algebraic connectivity

Viewing ω_i and K_{ij} as control variables, we aim at maximizing $\lambda_2(L(\theta^*))$ in order to improve the stability of both Eqs. (1) and (4). We first derive the variation of state algebraic connectivity due to change of natural frequency. We assume that the state algebraic connectivity is nondegenerate throughout optimization, which usually holds when the corresponding graph algebraic connectivity $\lambda_2(L[K])$ is nondegenerate.

There is no explicit expression of $\lambda_2(L(\theta^*))$. Nevertheless, it is possible to derive its derivatives using the perturbation theory, as commonly practiced in quantum mechanics. In the case that $\lambda_2(L_(\theta^*))$ is nondegenerate, the variation of $\lambda_2(L(\theta^*))$ is given by [16]

$$\begin{aligned}\delta\lambda_2(L(\theta^*)) &= \langle v_2(\theta^*)|\delta L(\theta^*)|v_2(\theta^*)\rangle \\ &= v_2(\theta^*)^T\,\delta L(\theta^*)\,v_2(\theta^*),\end{aligned} \qquad (6)$$

where $v_2(\theta^*)$ is the normalized eigenvector of $L(\theta^*)$ corresponding to $\lambda_2(L(\theta^*))$. Since $L(\theta^*)$ is a Laplacian matrix with edge weight $W(\theta^*)_{ij} = K_{ij}\cos(\theta_j^* - \theta_i^*)$, one has $\delta L(\theta^*)_{ij} = \delta_{ij}\sum_l \delta W(\theta^*)_{il} - \delta W(\theta^*)_{ij}$ and

$$\delta\lambda_2(L(\theta^*)) = \sum_{(i,j)} \delta W(\theta^*)_{ij}[v_2(\theta^*)_i - v_2(\theta^*)_j]^2. \qquad (7)$$

So the gradient of the state algebraic connectivity with respect to ω is

$$[\nabla_\omega\lambda_2(L(\theta^*))]_k = \sum_{(i,j)} \frac{\delta W(\theta^*)_{ij}}{\delta\omega_k}[v_2(\theta^*)_i - v_2(\theta^*)_j]^2. \qquad (8)$$

The computational complexity comes from the implicit dependence between shift of steady state $\delta\theta^*$ and change of natural frequency $\delta\omega$. In Ref. [13], $\delta\theta^*/\delta\omega$ is proved to be related to the pseudoinverse of $L(\theta^*)$. These expressions lead to a gradient ascent method to maximize $\lambda_2(L(\theta^*))$ by scheduling ω. However, this method requires solving the steady-state Eq. (2) and computing the pseudoinverse of $L(\theta^*)$ in every iteration, both of which are time consuming. In addition, convergence to the optimal solution can be very slow for gradient ascent update. In this paper, we propose to use the cut-set space approximation to simplify the problems as follows.

B. Cut-set space approximation of network flows

The natural frequency ω_i can be viewed as supply or demand of node i in a supply network as P_i in the power grid, and $K_{ij}\sin(\theta_j - \theta_i)$ is the resource or power transported from node j to node i. The steady-state Eq. (2) implies the flow conservation on each node.

Solving the nonlinear steady-state equation can be computationally costly. Recently, it has been shown that the cut-set space approximation of power flows can be rather

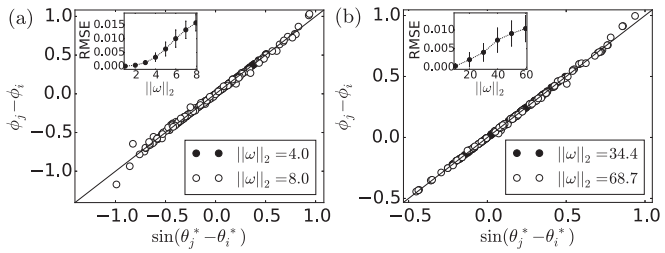

FIG. 1. $\phi_j - \phi_i$ vs. $\sin(\theta_j^* - \theta_i^*)$. (a) Erdös-Rényi graph of 50 nodes (ER50), where ω is drawn from a Gaussian distribution and $K_{ij} = 1$. Inset: root-mean-square error (RMSE) of estimator $\phi_j - \phi_i$ for $\sin(\theta_j^* - \theta_i^*)$ among all the edges. Each data point is averaged over 100 samples. (b) IEEE reliability test system 96 (RTS96) [19], where ω is modified from the power injection data in the test system and K_{ij} is defined to be the inverse of line reactance of edge (i, j). Inset: RMSE of estimator $\phi_j - \phi_i$ for $\sin(\theta_j^* - \theta_i^*)$ among all the edges. Each data point is averaged over 100 samples.

accurate in many regimes [15,17]. For completeness, the main steps are outlined as follows. We first formally rewrite the antisymmetric quantity $\sin(\theta_j^* - \theta_i^*)$ as $\beta_{ij} (= -\beta_{ji})$, which we try to decompose into the sum of two parts $\beta_{ij} = \beta_{ij}^{\text{cut}} + \beta_{ij}^{\text{cycle}}$. The first part β_{ij}^{cut} is expressed by the potential difference $\beta_{ij}^{\text{cut}} = \phi_j - \phi_i$, where ϕ_i is an unknown potential function to be solved self-consistently. The second part $\beta_{ij}^{\text{cycle}}$ satisfies the circular flow relation $\sum_{j\in\partial i} K_{ij}\beta_{ij}^{\text{cycle}} = 0\,\forall i$. In the language of graph theory, β^{cut} and β^{cycle} are said to live in the cut-set space and cycle space, respectively [15,18]. Substituting $\beta_{ij} = \phi_j - \phi_i + \beta_{ij}^{\text{cycle}}$ into Eq. (2), we have

$$\begin{aligned} 0 &= \omega_i + \sum_{j\in\partial i} K_{ij}\left(\phi_j - \phi_i + \beta_{ij}^{\text{cycle}}\right) \\ &= \omega_i - \sum_{j\in\partial i} L[K]_{ij}\phi_j, \end{aligned} \tag{9}$$

where $L[K]$ is the graph Laplacian matrix, which depends only on the network topology and edge weights. By taking the pseudoinverse of $L[K]$, denoted as $L[K]^\dagger$, the potential ϕ is obtained by $\phi = L[K]^\dagger\omega$, and subsequently, $\beta_{ij}^{\text{cut}} = \phi_j - \phi_i = \sum_l (L[K]_{jl}^\dagger - L[K]_{il}^\dagger)\omega_l$. It turns out that ϕ coincides with the DC approximation of AC power flow in power engineering θ^{DC} [15]. To simplify the calculation, it is proposed to approximate β by its cut-set space component β^{cut}, i.e., $\sin(\theta_j^* - \theta_i^*) \approx \phi_j - \phi_i = \sum_l (L[K]_{jl}^\dagger - L[K]_{il}^\dagger)\omega_l$.

Such an approximation is exact in some specific systems, such as acyclic graphs and systems with cut-set-inducing frequencies, while it has also been tested numerically in many generic networks that the approximation is surprisingly accurate [15,17]. We demonstrate two examples in Fig. 1. To quantify the stress of the system, the L^2 norm (or the Euclidean norm) of the natural frequency is used, i.e., $\|\omega\|_2 := \sqrt{\sum_i \omega_i^2}$. It is shown that the potential difference $\phi_j - \phi_i$ approximates $\sin(\theta_j^* - \theta_i^*)$ quite well even in the stress cases with large $\|\omega\|_2$.

C. Optimization by tuning natural frequencies

With the cut-set-space approximation, the edge weight of the state-dependent Laplacian matrix $L(\theta^*)$ can be approximated as

$$\begin{aligned} W(\theta^*)_{ij} &= K_{ij}\cos(\theta_j^* - \theta_i^*) = K_{ij}\sqrt{1 - \sin^2(\theta_j^* - \theta_i^*)} \\ &\approx \tilde{W}(\phi)_{ij} = K_{ij}\sqrt{1 - (\phi_j - \phi_i)^2} \\ &\equiv K_{ij}\sqrt{1 - \sum_{kl}\omega_k A_{kl}^{(ij)}\omega_l}, \end{aligned}$$

where $A^{(ij)}$ is defined to be a matrix with entry $A_{kl}^{(ij)} = (L[K]_{jk}^\dagger - L[K]_{ik}^\dagger)(L[K]_{jl}^\dagger - L[K]_{il}^\dagger)$ and we have made use of the fact that $\phi = L[K]^\dagger\omega$. Provided that $L[K]^\dagger$ is calculated and recorded, every time we calculate $W(\theta^*)$ we only need to solve for ϕ by simple matrix multiplication instead of solving the nonlinear steady-state equation Eq. (2). Now we work on the state algebraic connectivity $\lambda_2(\tilde{L}(\phi))$, which corresponds to the state-dependent Laplacian matrix with edge weight $\tilde{W}(\phi)_{ij} = K_{ij}\sqrt{1 - \sum_{kl}\omega_k A_{kl}^{(ij)}\omega_l}$. We assume in the following discussion that $|\phi_j - \phi_i| < 1$ always holds such that $\tilde{W}(\phi)_{ij}$ is real for every edge (i, j). This assumption can fail when the system is so stressed that $|\theta_j^* - \theta_i^*|$ is close to $\pi/2$ along some edges, in which case a preprocess to destress the system before optimization is needed.

The gradient in Eq. (8) can be estimated by $\nabla_\omega\lambda_2(\tilde{L}(\phi))$

$$[\nabla_\omega\lambda_2(\tilde{L}(\phi))]_k = \sum_{(i,j)} K_{ij}\frac{-\sum_l A_{kl}^{(ij)}\omega_l}{\sqrt{1 - \omega^T A^{(ij)}\omega}}[v_2(\phi)_i - v_2(\phi)_j]^2, \tag{10}$$

where $v_2(\phi)$ is the normalized eigenvector corresponding to $\lambda_2(\tilde{L}(\phi))$.

Similarly, the Hessian of the state algebraic connectivity is estimated by

$$\begin{aligned} H_{kl} = \frac{\partial^2\lambda_2(\tilde{L}(\phi))}{\partial\omega_k\partial\omega_l} &= \sum_{(i,j)}\frac{\partial^2\tilde{W}(\phi)_{ij}}{\partial\omega_k\partial\omega_l}[v_2(\phi)_i - v_2(\phi)_j]^2 \\ &+ \sum_{(i,j)} 2\frac{\partial W(\tilde{\phi})_{ij}}{\partial\omega_k}[v_2(\phi)_i - v_2(\phi)_j]\left[\frac{\partial v_2(\phi)_i}{\partial\omega_l} - \frac{\partial v_2(\phi)_j}{\partial\omega_l}\right], \end{aligned}$$

where $\partial v_2(\phi)/\partial\omega$ can also be obtained from the nondegenerate perturbation theory, which is computationally costly. We found in all our numerical experiments that truncating the second term of the Hessian can still lead to efficient optimization but simplify the calculation significantly. Hence, in the following we use the approximated Hessian $H_{kl} \approx \sum_{(i,j)}\partial^2\tilde{W}(\phi)_{ij}/\partial\omega_k\partial\omega_l[v_2(\phi)_i - v_2(\phi)_j]^2$ for optimization.

Obtaining the gradient and Hessian, we can define the update direction of gradient ascent and quasi-Newton method to maximize $\lambda_2(\tilde{L}(\phi))$,

$$\begin{aligned} \Delta\omega^{\text{gradient}} &= \nabla_\omega\lambda_2(\tilde{L}(\phi)), \\ \Delta\omega^{\text{Newton}} &= H^{-1}\nabla_\omega\lambda_2(\tilde{L}(\phi)). \end{aligned}$$

The natural frequency is updated by $\omega \leftarrow \omega + s\Delta\omega^{\text{gradient}}$ or $\omega \leftarrow \omega + s\Delta\omega^{\text{Newton}}$ with the step size s determined by backtracking line search [20], after which ω is enforced to be

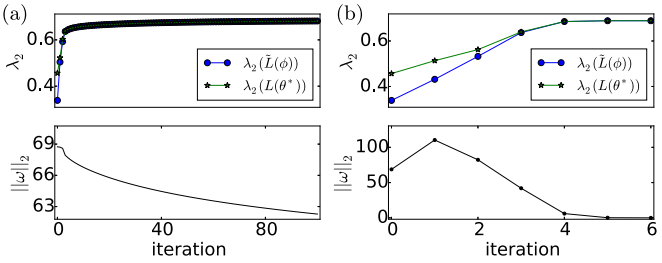

FIG. 2. λ_2 and $\|\omega\|_2$ through optimization for RTS96 power network. The initial natural frequency is modified from the power injection data in the test case. (a) Gradient ascent update. Both $\lambda_2(\tilde{L}(\phi))$ and $\lambda_2(L(\theta^*))$ increase gently in the later stage, and the natural frequency ω is approaching the optimal state $\omega = 0$ very slowly due to the flat landscape. (b) Quasi-Newton update. Both $\lambda_2(\tilde{L}(\phi))$ and $\lambda_2(L(\theta^*))$ approach the optimum $\lambda_2(L(\theta^* = 0)) = 0.6889$ after six iterations.

zero-sum by $\omega_i \leftarrow \omega_i - 1/N \sum_j \omega_j$ so that it admits a steady state.

In general, $\lambda_2(\tilde{L}(\phi))$ is an increasing function with $\tilde{W}(\phi)_{ij}$, which favors small phase angle difference across each edge. Without imposing any constraint, the optimal solution should take place at $\omega = 0$, in which case the optimum $\lambda_2(L(\theta^* = 0))$ coincides with the graph algebraic connectivity. In Fig. 2 we show the the optimization process for the RTS96 power network with gradient ascent update and quasi-Newton update. It is observed in this case that (i) $\lambda_2(\tilde{L}(\phi))$ is close to the exact state algebraic connectivity $\lambda_2(L(\theta^*))$ at the same ω [obtained by solving the steady-state Eq. (2) with ω given at that iteration]; (ii) the Newton's method is much more efficient than the gradient ascent, approaching the optimum within only a few steps, despite the extra efforts for computing the Hessian H and solving the linear equation $H\Delta\omega^{\text{Newton}} = \nabla_\omega \lambda_2(\tilde{L}(\phi))$ to obtain $\Delta\omega^{\text{Newton}}$. By taking the advantages of the cut-set space approximation and the Newton's method, our approach here provides a much more efficient algorithm compared to the previous study that relied on the full calculation of the nonlinear steady state and the gradient ascent update [13].

D. Optimization by tuning for coupling strengths

Instead of optimizing the natural frequencies, one can also tune the coupling strengths of edges to improve the stability. In power grids, this corresponds to the change of line reactance of each edge, which may be implemented by tuning the transmission lines or using FACTS devices [21]. Similarly, we can also derive the gradient and Hessian of $\lambda(\tilde{L}(\phi))$ with respect to the coupling strength

$$
\begin{aligned}
[\nabla_K \lambda_2(\tilde{L}(\phi))]_{(k,l)} &= \sum_{(i,j)} \frac{\delta \tilde{W}(\phi)_{ij}}{\delta K_{kl}} [v_2(\phi)_i - v_2(\phi)_j]^2 \\
&= \sum_{(i,j)} \Bigg\{ \delta_{(i,j),(k,l)} \sqrt{1 - \omega^T A^{(ij)} \omega} \\
&\quad + \frac{1}{2} K_{ij} \frac{-\sum_{mn} \omega_m \frac{\partial A^{(ij)}_{mn}}{\partial K_{kl}} \omega_n}{\sqrt{1 - \omega^T A^{(ij)} \omega}} \Bigg\} \\
&\quad \times [v_2(\phi)_i - v_2(\phi)_j]^2, \qquad (11)
\end{aligned}
$$

where the evaluation of $\partial A^{(ij)}/\partial K_{kl}$ relies on the computation of $\partial L[K]^\dagger/\partial K_{kl}$, which is attainable as long as the rank of $L[K]$ remains unchanged [22]. The gradient ascent update is simply given by $K \leftarrow K + s\nabla_K \lambda_2(\tilde{L}(\phi))$. The Hessian matrix and update of Newton's method can also be obtained straightforwardly, although the expression is extremely tedious. The update of coupling strength renders the modification of $L[K]$ and recalculation of $L[K]^\dagger$, making it much more time consuming than the update of natural frequencies.

Although we have been dealing with the oscillatory system with sinusoidal coupling, we remark that the general framework developed here can also be applicable to systems with other coupling functions, and even other eigenvalue optimization problems, especially when nonlinearity comes into play and the usual semidefinite programming is not directly applicable [20].

IV. RESULTS

A. Behavior at optimal natural frequencies

To obtain a nontrivial solution with optimal stability, we introduce an additional Euclidean norm constraint,

$$\|\omega\|_2^2 = \sum_i \omega_i^2 \geqslant c, \qquad (12)$$

which treats all nodes in equal footing and doesn't emphasize the role of import nodes, say, hubs. The constraint optimization is solved by the barrier method, which is a particular interior point algorithm [20]. Although the constraint Eq. (12) is nonconvex and global optimum may not be attainable, we find in our numerical experiments that the barrier method can efficiently achieve a satisfactory stationary point.

In Fig. 3(a) we plot the optimization process of the RTS96 power network with constraint parameter $c = 0.99\|\omega_0\|_2^2$, where ω_0 is the same as the initial natural frequency in Fig. 2. The corresponding unoptimized and optimized system is shown in Fig. 3(b). The edge (318,223) and edge (325,121) are the interconnections between two components. In the extreme case, if both of them are overloaded with $|\theta_i^* - \theta_j^*| = \pi/2$ or $\cos(\theta_i^* - \theta_j^*) = 0$, then the metagraph with edge weight $W(\theta^*)_{ij}$ becomes disconnected into two parts, and $\lambda_2(L(\theta^*))$ will become zero, signaling the onset of instability of the system [12,23]. In our case, edge (325,121) is heavily loaded in the unoptimized system, while it is significantly destressed in the optimized system, achieving a more stable state as revealed by the increment of $\lambda_2(L(\theta^*))$.

To illustrate the improved stability of the optimized system related to an unoptimized one, we impose a small disturbance δ_i to the steady state at $t = 0$, $\theta_i(t = 0) = \theta_i^* + \delta_i$ and let the system evolve according to both the first- and second-order Kuramoto model. In Figs. 3(c) and 3(d) we monitor the discrepancy between $\theta(t)$ and the steady state $\varepsilon(t) := \sum_i |\theta_i(t) - \theta_i^*|$. It is observed that the optimized system converges to the steady state more rapidly than the unoptimized system.

B. Properties of optimized systems

In the following, we explore some general properties of the optimal systems under the Euclidean norm constraint. The networks are ER random graphs with 50 nodes and every pair

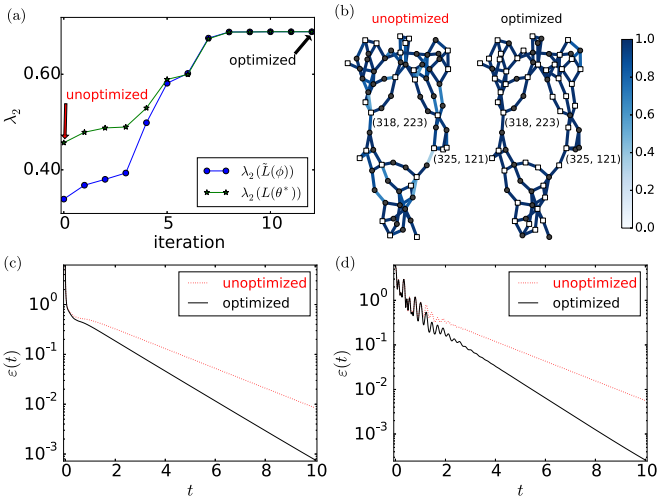

FIG. 3. (a) λ_2 through optimization for the RTS96 power network under Euclidean norm constraint. (b) The unoptimized and optimized system, where white square nodes have positive natural frequencies (generators) while gray circular nodes have nonpositive natural frequencies (loads or relay nodes). Edge color intensity encodes $\cos(\theta_i^* - \theta_j^*)$. (c) Response of the RTS 96 power network governed by the first-order Kuramoto model. (d) Response of the RTS 96 power network governed by the second-order Kuramoto model with unit damping $D_i = 1$ and small inertia $M_i = 0.2$. In both (c) and (d), the disturbance, drawn from the Gaussian distribution with mean zero and standard deviation 0.05 rad, was applied to the steady state of phase oscillators at $t = 0$.

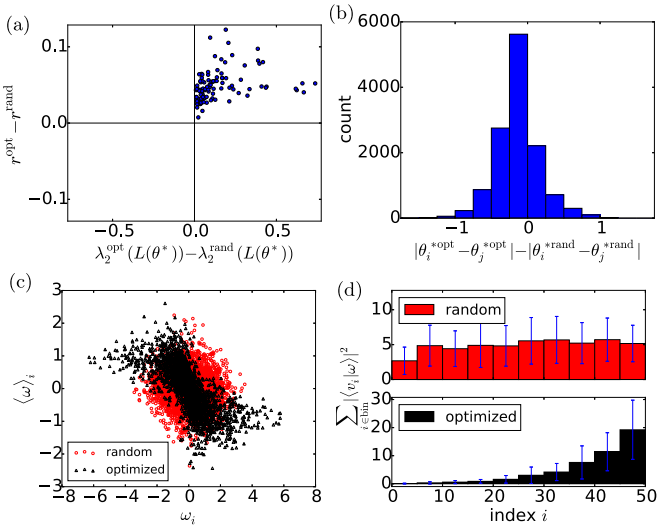

FIG. 4. Properties of the optimal system compared to systems with random frequencies. The networks are 100 realizations of ER random graphs with 50 nodes and edge connection probability $p = 0.1$. (a) Correlation of increment of $\lambda_2(L(\theta^*))$ and order parameter r. (b) Histogram of changes of phase angle differences among all edges (i, j) in all realizations. (c) Average neighbor frequency $\langle\omega\rangle_i = \sum_{j\in\partial i}\omega_j/d_i$ vs. natural frequency ω_i. (d) Alignments of natural frequencies with graph Laplacian eigenvectors, i.e., $|\langle v_i|\omega\rangle|^2$ where v_i is the normalized eigenvector corresponding to the ith smallest eigenvalue. The data was divided into 10 bins and $|\langle v_i|\omega\rangle|^2$ was first summed inside every bin for each sample, after which the sample mean and standard deviation of the bin summation quantity $\sum_{i\in\rm bin}|\langle v_i|\omega\rangle|^2$ was calculated.

of nodes are connected with probability $p = 0.1$. As found in Fig. 4(a), not only does the optimization result in improving the objective function $\lambda_2(L(\theta^*))$, but also the Kuramoto order parameter $r := N^{-1}|\sum_j e^{i\theta_j^*}|$. In fact, more coherent phase angles in general imply smaller phase angle differences $|\theta_i^* - \theta_j^*|$ and larger edge weight $W(\theta^*)_{ij} = K_{ij}\cos(\theta_i^* - \theta_j^*)$, in which case the state-dependent network will be better connected with a higher algebraic connectivity. Thus, it is not surprising that there is a correlation between the enhancements of r and $\lambda_2(L(\theta^*))$. We show in Fig. 4(b) that the decrease of phase angle differences $|\theta_i^* - \theta_j^*|$ after optimization is much more common than increase.

It is found in previous studies that natural frequencies which optimize r subject to constraint of the form $\|\omega\|_2^2 =$ constant have negative correlations between neighboring frequencies, and align with eigenvectors corresponding to large eigenvalues of graph Laplacian [24]. We show in Figs. 4(c) and 4(d) that such properties are also observed in natural frequencies, which optimize $\lambda_2(L(\theta^*))$. In the case of power grids on such networks, the negative correlations between neighboring frequencies at the optimum imply that a supply node ($\omega_i > 0$) is more likely to be connected to demand nodes ($\omega_i < 0$) and viceversa. This indicates that the system stability favors distributed power sources if all the nodes are not constrained, which is similar to the phenomenon observed in Ref. [25] that decentralized power grids promote synchrony.

However, the pathways of achieving optimality with decentralized networks are different. In Ref. [24] decentralization was achieved by maximizing the overlap of the configuration with the eigenvector of the *largest* eigenvalue of the graph Laplacian matrix, whereas in our work, optimal stability is achieved by maximizing the *smallest* positive eigenvalue of the state-dependent Laplacian matrix.

Further insight can be obtained from the alignments of optimal frequencies or power injections with the eigenvectors of *graph Laplacian matrix* $L[K]$. We depict in Figs. 5(a) and 5(b) the eigenvectors corresponding to the second smallest and largest eigenvalues of $L[K]$ of an ER graph, denoted as v_2 and v_N. In Fig. 5(a), the network is partitioned into two connected subgraphs by v_2, with the positive components of v_2 belonging to one subgraph and the negative components belonging to the other, and there are only limited number of edges connecting them. It constitutes an example of graph bipartition by spectral method [26,27]. If the power injection is aligned with v_2, i.e., $\omega \propto v_2$, then the implication is an extensive transportation of resources from one group to the other, as illustrated by the large phase difference across the link (325,121) in Fig. 3(b), rendering the boundary between the two groups vulnerable. On the contrary, as shown in Fig. 5(b), the subset of positive components of v_N (white) is maximally connected to the subset of negative components (gray), yielding a decentralized configuration. The observed suppression of alignment of ω with v_2 in Fig. 4(d) in the optimized systems implies that the domain-wide fluctuations of resource or power is inhibited to enhance stability after optimization. On the other hand, the alignment of ω with v_N

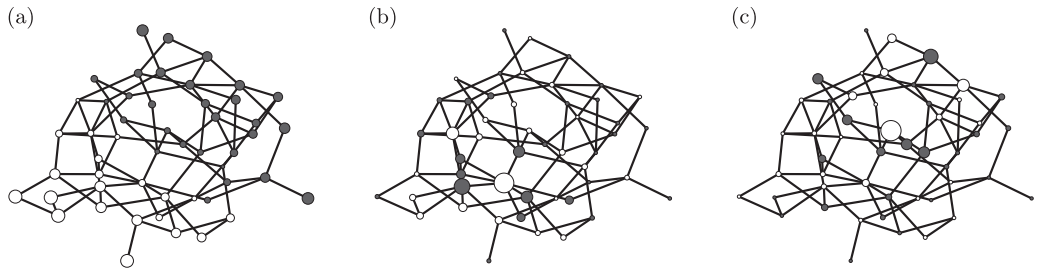

FIG. 5. (a) Eigenvector v_2 corresponding to the second smallest eigenvalue λ_2 of the graph Laplacian matrix of a specific ER random graph, depicted on the network. The color indicates the sign of v_{2j} on node j, i.e., white node corresponds to $v_{2j} > 0$, while gray node corresponds to $v_{2j} \leqslant 0$. The size of the node indicates the strength of $|v_{2j}|$ on that node. (b) Eigenvector v_N corresponding to the largest eigenvalue λ_N of the graph Laplacian matrix depicted on the network. (c) Frequencies ω^{opt} corresponding to the algebraic connectivity of the state-dependent Laplacian matrix evaluated at the optimal algebraic connectivity. Similarly, the white nodes correspond to $\omega^{\text{opt}} > 0$, while the gray nodes correspond to $\omega^{\text{opt}} \leqslant 0$.

is enhanced, which implies that the optimization of the system stability encourages local transmission. As shown in Fig. 5(c), power injection on the white nodes tends to have distributed power sources.

C. Difference between $\lambda_2(L(\theta^*))$ and r

Observing the similarity of the results of optimizing $\lambda_2(L(\theta^*))$ with the Euclidean norm constraint and those of optimizing r with the same constraint, it is tempting to conclude that the more synchronized a system the more stable it is and one can improve the system stability by just increasing the order parameter r, which can be much simpler. However, we argue that while such a judgment is valid in many cases like the above homogeneous ER graphs, it is not necessarily a universal rule. In most cases, optimizing r will not be the most efficient way to enhance the system stability. Moreover, there is a conceptual difference between the two quantities. The Kuramoto order parameter r is a measure of coherence of phase angles of all oscillators in a global and average sense, which cannot identify the role of critical edges in maintaining stability, e.g., the interconnections between modules. To be more concrete, we consider a simple network which is composed of two modules, each corresponding to a small random graph, as sketched in Fig. 6(b). The coupling of each edge is set to be $K_{ij} = 1$.

In Case 1, we suppress the intramodule transportation and encourage the intermodule transportation, which leads to phases that are coherent inside each module but have a large separation between the two modules, as shown in Fig. 6(a). The phase coherence inside each module leads to a relatively high Kuramoto order parameter $r = 0.823$. However, the large intermodule phase difference indicates the edge (0,15) and edge (1,16) are highly stressed with a low state dependent edge weight $W(\theta^*)_{ij} = K_{ij}\cos(\theta_i^* - \theta_j^*)$, resulting in a small state algebraic connectivity $\lambda_2(L(\theta^*)) = 0.058$ as shown in Fig. 6(b). In Case 2, the system is perturbed and the phases become more dispersed, leading to a smaller Kuramoto order parameter $r = 0.725$. But the phase differences along edge (0,15) and edge (1,16) are much reduced. This significantly increases the edge weights $W(\theta^*)_{ij}$ of these two edges and hence the state algebraic connectivity reaches $\lambda_2(L(\theta^*)) = 0.151$, since edge (1,15) and edge (1,16) are the intermodule connections whose edge weights are crucial for the algebraic connectivity. This simple example highlights the essence of using $\lambda_2(L(\theta^*))$ as a cost function for measuring stability in general networks.

D. Inclusion of practical power grid constraints

The Euclidean norm-constrained optimization problem above treats all nodes on equal footing where a supplier can become a consumer and vice versa. This will not be realistic if we consider power-grid applications. In this section, we consider two problems regarding practical constraints of power grid operations.

In Problem 1, both the supply and the demand are restricted to vary within a certain range. Furthermore, regulating both the generation and consumption may be necessary in future grids with the introduction of renewable energy. Hence specifically

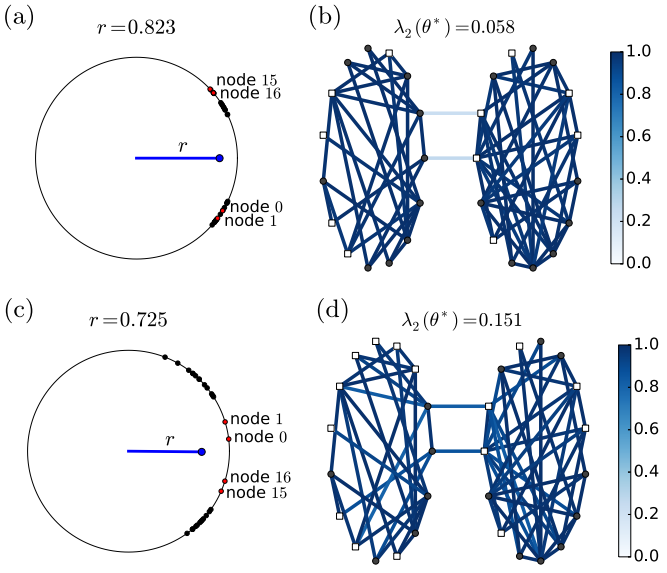

FIG. 6. Phase angles θ^* and state-dependent edge weights $W(\theta^*)$ in a two-module network. In both cases, the L^2-norm of natural frequency is $\|\omega\|_2 = 4.26$. (a) Phases of the system depicted on the unit circle in Case 1. (b) The state-dependent edge weight $W(\theta^*)_{ij} = K_{ij}\cos(\theta_i^* - \theta_j^*)$ in Case 1. (c) Phases of the system depicted on the unit circle in Case 2. (d) The state-dependent edge weight $W(\theta^*)_{ij} = K_{ij}\cos(\theta_i^* - \theta_j^*)$ in Case 2.

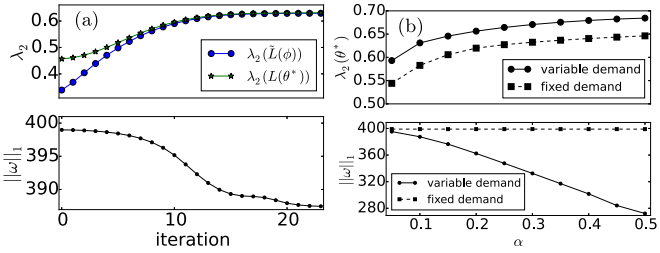

FIG. 7. (a) λ_2 and $\|\omega\|_1$ through optimization for the RTS96 power network under linear constraints at $\alpha = 0.1$. The L_1-norm of natural frequency $\|\omega\|_1 := \sum_i |\omega_i|$ is twice of total generation or total consumption. (b) $\lambda_2(L(\theta^*))$ and $\|\omega\|_1$ of the optimal system as a function of α with variable demand (Problem 1) and fixed demand (Problem 2).

we consider the constraint $\omega_{0i} - \alpha|\omega_{0i}| \leqslant \omega_i \leqslant \omega_{0i} + \alpha|\omega_{0i}|$ for i to be either a supply node or demand node, where ω_{0i} is the natural frequency of the original system and the parameter α satisfies $0 < \alpha \leqslant 1$. For the relay node with $\omega_{0i} = 0$, the natural frequency will remain unchanged throughout optimization $\omega_i = \omega_{0i} = 0$.

In Problem 2, only the supply nodes with $\omega_{0i} > 0$ are allowed to schedule their productions with fraction α, while the demands must be satisfied and the relay nodes should also be fixed, i.e., $\omega_i = \omega_{0i}$ for $\omega_{0i} \leqslant 0$. To deal with both the inequality and equality constraints, the primal-dual interior point method in convex optimization is applied in these problems. Although we always make the supply and demand balanced in every iteration, we discovered that imposing the additional constraint $\sum_i \omega_i = 0$ into the definition of the problem can significantly facilitate the convergence of the algorithm.

In Fig. 7(a), we plot the optimization process of the RTS96 power network with constraints of Problem 1. The primal-dual interior point algorithm can bring the system to optimum effectively. We also monitor the L^1-norm of ω, defined as $\|\omega\|_1 := \sum_i |\omega_i|$, which is twice the total production or total consumption. During optimization, the system is also destressed as indicated by the decrement of $\|\omega\|_1$. In Fig. 7(b), we plot $\lambda_2(L(\theta^*))$ and $\|\omega\|_1$ as a function of α with constraints of both Problem 1 and Problem 2. It is observed that $\lambda_2(L(\theta^*))$ increases with α for both cases with variable demands and fixed demands. This is not surprising since the feasible region of the problem with larger α is a superset of the one with smaller α, and a larger feasible region gives the system more flexibility to search for more stable state. The system can achieve higher stability with variable demands in Problem 1 than the fixed demand in Problem 2, which is also due to more degrees of freedom to vary in Problem 1. Our method can solve both problems satisfactorily.

E. Behavior at optimal coupling strengths

Last, we consider behavior at the optimal state algebraic connectivity by updating the coupling strengths. To avoid indefinite solutions, we impose a simple constraint,

$$\sum_{(i,j)} K_{ij} = K_{\text{total}}, \tag{13}$$

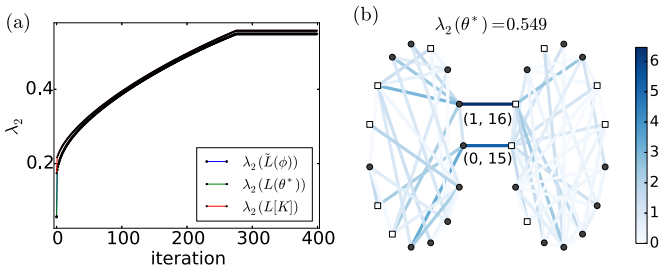

FIG. 8. Optimizing the state algebraic connectivity by updating coupling strengths. (a) State algebraic connectivity $\lambda_2(L(\theta^*))$, $\lambda_2(\tilde{L}(\phi))$, and graph algebraic connectivity $\lambda_2(L[K])$ through optimization. The initial state is the same as Case 1 in Sec. IV C. (b) The state-dependent edge weight $W(\theta^*)_{ij} = K_{ij}\cos(\theta_i^* - \theta_j^*)$ in the optimal state. Note the scale of color code is different from the cases of Fig. 6.

where K_{total} represents the availability of the total capacity, and K_{ij} is constrained to be nonnegative. Due to the high complexity of computing the Hessian, we only consider the gradient ascent update. To preserve the resource constraint, the approximated gradient $\nabla_K \lambda_2(\tilde{L}(\phi))$ as calculated by Eq. (11) is projected onto the feasible region, after which the coupling strengths are updated. In Fig. 8(a), we plot the optimization process of the projected gradient update on the two-module network discussed in Sec. IV C, and the initial condition is the same as Case 1 in Sec. IV C. It is shown that redistributing the coupling strengths can significantly improve both the graph algebraic connectivity and state-algebraic connectivity, reaching a more stable state. In Fig. 8(b), we sketch the state-dependent edge weight in the optimal state. Contrary to the unoptimized system in Fig. 6(b), the optimized system exhibits large edge weight $W(\theta^*)_{ij}$ in edge (1,16) and edge (0,15), the interconnections between the two modules, which favors higher state algebraic connectivity. For each module, the nodes are well connected and the need for transporting resource is modest. Thus, the coupling strengths inside each module are sacrificed so that the system can invest more on the the critical edges. The effects of increasing stability by investments on the interarea links are also studied and demonstrated in Ref. [28], where the interlinks are added one by one according to the greedy search strategy instead of updating the existing links as in our approach. These phenomena highlight the importance of strengthening the interconnections between different communities of the grid.

V. DISCUSSION

In this paper, we studied the optimization of synchronization stability of the Kuramoto model by updating the natural frequencies or coupling strengths. The proposed cut-set space approximation can accurately estimate the network flows of steady states and thus simplify the objective function, i.e., the state algebraic connectivity whose increment can increase the stability of the phase-locked steady states of both the first- and second-order Kuramoto model. Such an approximation leads to compact expressions of gradient and Hessian of the cost function. Together with the interior point algorithm or projected gradient ascent, our method can cope with various

constraints, which is shown to be effective and efficient. There is a general correlation between the optimization of the Kuramoto order parameter and the state algebraic connectivity, especially in the homogeneous networks. However, the Kuramoto order parameter cannot represent the role of critical links, e.g., intermodule connections, which is crucial to the synchronization stability. In light of this consideration, the state algebraic connectivity is a more appropriate cost function for the measure of stability. Our framework has potential applications in improving the stability of power grids which are usually simplified to a second-order Kuramoto model. The method also sheds light on the treatments of general nonlinear eigenvalue optimization problems.

Nevertheless, there are many other aspects to consider concerning the application of power grids, such as extending our formalism to nonuniform inertia or damping, lossy transmissions, effect of changes of network topology due to breakdown of grid elements, etc. In addition, our method is based on the assumption of nondegenerate state algebraic connectivity, which may not hold in highly symmetric networks, and how to achieve an optimum under general constraints in these networks remains to be explored. Last, our study considers only linear stability which assumes small disturbances. While we found that the decentralized configuration has optimal stability for small disturbances, there were indications that decentralization may reduce the dynamic stability for moderate perturbations [25]. This may require us to adopt an augmented objective function in future studies. The recently developed basin stability approach [29] can be complementary to our approach, and the combination of the two views may be able to provide more comprehensive understanding of the system stability.

ACKNOWLEDGMENTS

We are grateful to D. Saad, H. Wang, P. Choi, M. Yan, H. Tsang, and X. Huang for fruitful discussions. This work is supported by grants from the Research Grants Council of Hong Kong (Grants No. 605813 and No. 16322616).

[1] S. Strogatz, *Sync: How Order Emerges from Chaos in the Universe, Nature, and Daily Life* (Hyperion Books, New York, 2004).
[2] A. Pikovsky, M. Rosenblum, and J. Kurths, *Synchronization: A Universal Concept in Nonlinear Sciences*, Cambridge Nonlinear Science Series (Cambridge University Press, Cambridge, 2003).
[3] J. A. Acebrón, L. L. Bonilla, C. J. Pérez Vicente, F. Ritort, and R. Spigler, Rev. Mod. Phys. **77**, 137 (2005).
[4] P. Kundur, *Power System Stability And Control*, EPRI power system engineering series (McGraw-Hill Education, India, 1994).
[5] J. M. Carrasco, L. G. Franquelo, J. T. Bialasiewicz, E. Galvan, R. C. PortilloGuisado, M. A. M. Prats, J. I. Leon, and N. Moreno-Alfonso, IEEE Trans. Indus. Electron. **53**, 1002 (2006).
[6] S. Boccaletti, J. Kurths, G. Osipov, D. Valladares, and C. Zhou, Phys. Rep. **366**, 1 (2002).
[7] A. Arenas, A. Díaz-Guilera, J. Kurths, Y. Moreno, and C. Zhou, Phys. Rep. **469**, 93 (2008).
[8] F. A. Rodrigues, T. K. D. Peron, P. Ji, and J. Kurths, Phys. Rep. **610**, 1 (2016).
[9] L. M. Pecora and T. L. Carroll, Phys. Rev. Lett. **80**, 2109 (1998).
[10] D. Cvetković, W. Haemers, P. Rowlinson, and N. M. M. de Abreu, Linear Algebra Appl. **423**, 53 (2007).
[11] F. Chung, *Spectral Graph Theory*, CBMS Regional Conference Series No. 92 (Conference Board of the Mathematical Sciences, 1997).
[12] A. Araposthatis, S. Sastry, and P. Varaiya, Intl. J. Electrical Power Energy Syst. **3**, 115 (1981).
[13] E. Mallada and A. Tang, *50th IEEE Conference on Decision and Control and European Control Conference (CDC-ECC)* (IEEE, 2011), pp. 7729–7734.
[14] A. E. Motter, S. A. Myers, M. Anghel, and T. Nishikawa, Nat. Phys. **9**, 191 (2013).
[15] F. Dörfler, M. Chertkov, and F. Bullo, Proc. Natl. Acad. Sci. USA **110**, 2005 (2013).
[16] L. Landau and E. Lifshitz, *Quantum Mechanics: Nonrelativistic Theory* (Butterworth-Heinemann, London, 1977).
[17] F. Dörfler and F. Bullo, *Power and Energy Society General Meeting (PES)* (IEEE, 2013), pp. 1–5.
[18] N. Biggs, Bull. London Math. Soc. **29**, 641 (1997).
[19] C. Grigg, P. Wong, P. Albrecht, R. Allan, M. Bhavaraju, R. Billinton, Q. Chen, C. Fong, S. Haddad, S. Kuruganty, W. Li, R. Mukerji, D. Patton, N. Rau, D. Reppen, A. Schneider, M. Shahidehpour, and C. Singh, IEEE Trans. Power Syst. **14**, 1010 (1999).
[20] S. Boyd and L. Vandenberghe, *Convex Optimization*, Berichte über verteilte messysteme (Cambridge University Press, Cambridge, 2004).
[21] D. J. Gotham and G. T. Heydt, IEEE Trans. Power Syst. **13**, 60 (1998).
[22] V. P. G. H. Golub, SIAM J. Numer. Anal. **10**, 413 (1973).
[23] D. Manik, D. Witthaut, B. Schäfer, M. Matthiae, A. Sorge, M. Rohden, E. Katifori, and M. Timme, Eur. Phys. J. Special Topics **223**, 2527 (2014).
[24] P. S. Skardal, D. Taylor, and J. Sun, Phys. Rev. Lett. **113**, 144101 (2014).
[25] M. Rohden, A. Sorge, M. Timme, and D. Witthaut, Phys. Rev. Lett. **109**, 064101 (2012).
[26] M. Fiedler, Czechoslovak Math. J. **25**, 619 (1975).
[27] M. Holzrichter and S. Oliveira, *Parallel and Distributed Processing: Proceedings of the 11th IPPS/SPDP'99 Workshops Held in Conjunction with the 13th International Parallel Processing Symposium and 10th Symposium on Parallel and Distributed Processing San Juan, Puerto Rico, USA, April 12–16*, edited by José Rolim *et al.*, Lecture Notes in Computer Science Vol. 1586 (Springer, Berlin/Heidelberg, 1999), pp. 978–985.
[28] B. Wang, H. Suzuki, and K. Aihara, Sci. Rep. **6**, 26596 (2016).
[29] P. J. Menck, J. Heitzig, J. Kurths, and H. Joachim Schellnhuber, Nat. Commun. **5**, 3969 (2014).